Progress In Electromagnetics Research B, Vol. 47, 179–202, 2013

A MONTE-CARLO MPSTD ANALYSIS OF SCATTERING FROM CYLINDERS BURIED BELOW A RANDOM PERIODIC ROUGH SURFACE

Yueyang Dai, Wei Liu, and Xiaobang Xu*

Holcombe Department of Electrical and Computer Engineering, Clemson University, Clemson, SC 29634-0915, USA

Abstract—The analysis of scattering of objects buried below a random rough surface is of practical interest. In reality, the random rough surface may be of an extensive periodic structure. To deal with this more realistic situation, this paper presents a Monte-Carlo MPSTD numerical technique developed for investigating the scattering of a cylinder buried below a random periodic rough surface. The computation model is formulated in two steps. In the first step, only the random rough surface is considered and the periodic boundary condition (PBC) is enforced at the two ends of a period of the rough surface. Then, in the second step, a cylinder is placed below the random rough surface and the interaction between the buried cylinder and the rough surface is taken into account. In each of the two steps, the fields are computed employing the MPSTD algorithm developed in the authors' previous work. Sample numerical results are presented and validated.

1. INTRODUCTION

Over the last a few decades, significant research has been conducted on the analysis of electromagnetic scattering of buried object for its practical importance in both military and civil applications, such as subsurface investigation and target detection. In reality, the media interface may be a random rough surface, which could be of extensive periodic structure. It is important to incorporate the nature of the random rough surface in the electromagnetic scattering study because of its substantial impact on the scattered signal of the buried object.

To study the scattering of a buried object near a random rough surface, both analytical and numerical methods have been developed

Received 1 October 2012, Accepted 26 December 2012, Scheduled 2 January 2013

* Corresponding author: Xiaobang Xu (ecexu@clemson.edu).

in the frequency domain. An application of the small perturbation method (SPM) for studying the scattering is presented in [1]. For a numerical simulation of objects above or below a rough surface, integral equations have been formulated and solved by the method of moments (MoM) [2–9]. In particular, itwas employed together with a steepest-descent fast multipole method [4–7]; and in the analysis presented in [5, 8, 9], a layered structure was considered. Meanwhile, the finite element method (FEM) has been combined with Monte-Carlo method to study scattering from objects on a rough sea surface [10].

As an effective time-domain method, the Monte-Carlo finite-difference time-domain (FDTD) method has been developed to study this kind of scattering problems, including that of an object above a random periodic rough surface [11]. Being compared with the surface integral equation method, the FDTD approach is more effective for modeling inhomogeneous objects and complex geometries. And either pulsed or continuous wave (CW) illumination can be used, propagation of both the total and scattered fields can be observed in the time domain. However, this method has major drawbacks. As pointed out in [12, 13], the FDTD approach based on the classical Yee scheme with quadratic cell mapping in space gives the modeled structures a "staircase nature" and requires a number of grids per wavelength. Numerous numerical examples reported in the literature have verified that a fine discretization of 10–20 cells per minimum wavelength is required to obtain acceptable accuracy of solutions. Furthermore, the classical FDTD approach is ill-suited for arbitrary geometries with multiple materials.

Recently, the pseudospectral time-domain (PSTD) method has been developed and successfully applied to solve various problems of practical interest, such as determining the electromagnetic scattering by objects placed in an open space [14–21] and investigating the scattering of two-dimensional (2D) cylinders buried in a half space with a planar [22, 23] or an undulating surface [23]. This method has been systematically presented in [24]. As pointed out in [15], "The pseudospectral schemes can be thought of as a maximum order finite-difference schemes and as such takes the role of the royals among numerical schemes for the solution of partial differential equations. As we shall learn properly formulated pseudospectral schemes yield not only superior accuracy but does so in a very efficient manner as compared to low-order FDTD schemes." This has been demonstrated by a number of numerical experiment results reported in the literature [17, 22, 23]. Moreover, the spatial grid is not staggered like the one used in the classical FDTD Yee scheme, so that the derivation, programming and representation of materials are more

straightforward. This is extremely beneficial when a random rough surface is involved in the computation. Also, as indicated in [23], in contrast to the classical FDTD Yee scheme with the "staircase nature", the multidomain pseudospectral time-domain (MPSTD) approach is well suited for complicated geometries with a great flexibility. This nature warrants a good potential of the MPSTD method for application in the analysis of scattering involving random rough surfaces, the geometry of which is apparently complex and needs special attention. But to the best knowledge of the authors, the MPSTD method that is more effective than the classic FDTD approach had not been applied in combination with the Monte-Carlo method for determining the scattering of objects buried below a *random* rough surface, which may better simulate media interfaces in reality and is of practical interest, until most recent time.

Most recently, a Monte-Carlo MPSTD algorithm has been developed for investigating the scattering of a 2D cylinder buried below a random rough surface [25]. But the investigation is limited for a random rough surface of *finite* length.

However, in reality, a random rough surface may be of an extensive periodic structure. To take care of the more realistic situation, in this paper, the Monte-Carlo MPSTD algorithm presented in the authors' previous work [25] is further developed for studying the scattering of a 2D cylinder buried below a random periodic rough surface. One notes that due to the existence of the buried cylinder, the structure loses its periodic nature; and it is hard to compute the scattering in a finite computation domain by one step. To face this challenge, we propose a two-step MPSTD numerical technique. In the first step, only the random periodic rough surface is considered so that the periodic boundary condition (PBC) can still be used to simulate the extensive periodic rough surface. Then, in the second step, the near-zone field scattered by the *entire* periodic rough surface obtained in the first step is used as the excitation to the buried cylinder to determine the scattering from the buried cylinder and that due to the interaction between the cylinder and the rough surface. The length of a period of the periodic rough surface is taken to be much longer than the correlation length of the random rough surface and be sufficiently large compared with the dimension of the buried cylinder, then the computation can still be carried out in a finite computation domain as described in Section 3. The rest of this paper is organized as follows. In Section 2, we formulate the computation model for the scattering of a random periodic rough surface alone, where the periodic boundary condition (PBC) is enforced. Then, in Section 3, a cylinder buried below the random rough surface is considered and the computation

model is developed in two steps. Using the computation model, sample numerical results are obtained, presented, and validated in Section 4. Finally, conclusions are drawn in Section 5.

2. COMPUTATION MODEL FOR SCATTERING FROM A RANDOM PERIODIC ROUGH SURFACEALONE

2.1. Introduction to a Random Periodic Rough Surface

In the computation model for simulating the scattering of an extensive random rough surface, the rough surface must be artificially truncated at the two ends of the computation domain that is of finite length. This truncation would force the current on the rough surface to be zero at the truncation edges. Subsequently, such an abrupt change of surface current would cause artificial reflection from the two edges. To prevent the current discontinuity, a tapered incident wave has been introduced in spatial or spectral domain to make the excitation decay gradually and become negligible at the surface edges [26]. But as the incident angle increases, especially at low grazing angles, the

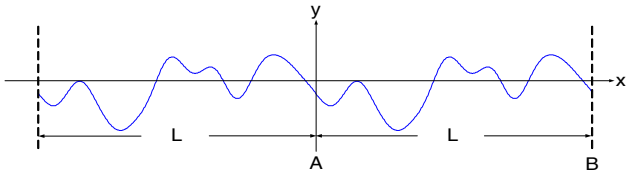

Figure 1. A random periodic rough surface.

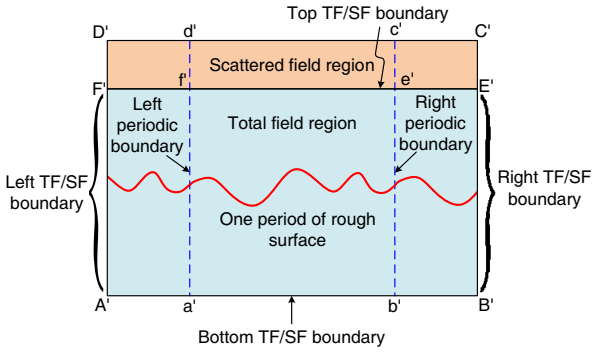

Figure 2. The computation domain for a random periodic rough surface alone (The first step).

illuminated area becomes large, which would require huge memory and cause complexity, making the numerical simulation difficult.

In this paper, we study an extensive random periodic rough surface shown in Fig. 1, where L is the length of one period. To simulate the statistic characteristics of the roughness of a random rough surface, L should be greater than several correlation lengths l_c and in general it is taken to be [27]

$$L \geq 15l_c. \tag{1}$$

Then the diffraction from the truncated edges can be eliminated by enforcing a periodic boundary condition (PBC) there [26, 28, 29]. According to the Floquet Theorem [30], by enforcing the PBC, the fields along an extensive periodic rough surface can be readily described by the fields in one period cell. In this way, only one period of rough surface needs to be included in the computation domain, which can significantly improve the computation efficiency.

2.2. Formulation of the Computation Model

The MPSTD computation domain for studying the scattering from a random periodic rough surface is depicted in Fig. 2. For simplicity, the perfectly matched layer (PML) [23–25] regions surrounding the "regular" region are not included there. As shown in this figure, the computation domain is divided into two regions: the total field region and the scattered field region. In the total field region enclosed by $A'B'E'F'$, the field is the sum of the incident field to the rough surface, which is the driving composite field described in [25], and the field scattered by the rough surface. In the scattered field region enclosed by $C'D'F'E'$, only the field scattered by the rough surface exists. The incident fields are injected at the four total-field/scattered-field (TF/SF) interfaces $A'F'$, $F'E'$, $E'B'$ and $B'A'$.

Also, as shown in Fig. 2, a period of rough surface is included in the computation domain. At its side boundaries $a'd'$ and $b'c'$, the periodic boundary conditions, for E_z as an example, are enforced [31],

$$E_z(x_{b'c'}, y, t) = E_z(x_{a'd'}, y, t - L/v_x), \tag{2a}$$

$$E_z(x_{a'd'}, y, t) = E_z(x_{b'c'}, y, t + L/v_x), \tag{2b}$$

where $v_x = v/\sin\theta$ is the phase velocity in x direction, and θ is the incident angle. At normal incidence, $\theta = 0$, we can simply set the nodal values of the fields on the periodic boundaries at left- and right-hand sides equal at every time step.

3. COMPUTATION MODEL FOR SCATTERING FROM BURIED CYLINDER BELOW RANDOM PERIODIC ROUGH SURFACE

After placing a cylinder below a random periodic rough surface, the structure is no longer periodic. Hence, the periodic boundary condition cannot be used anymore and the computation model must be modified. The new computation procedure is thus decomposed into two steps [11]. The key idea of the two-step approach is similar to that of a "three-wave" method presented in [32–34], which has been successfully used in the finite-difference time-domain (FDTD) analysis of scattering of an object buried below a planar media interface. As shown in [32], in such an FDTD analysis, first, the incident, reflected, and transmitted fields associated with the planar media interface are calculated in the absence of an object. Then, the calculated composite field (also called as the "three-wave" field), which is the sum of the incident and reflected field in the upper half space and the transmitted field in the lower half space, is employed as the driving field of an object near the interface to determine the scattering of the object and interface combination. It is indicated in [32] that in principle, the interface involved in this approach that consists of two steps may be of any geometry; but one understands that if the media interface is a random rough surface instead of a planar surface, the scattered field by the rough surface, rather than the reflected and transmitted field associated with a planar interface, should be calculated first. Based on this key idea, the computation presented in this paper is performed in two steps. In the first step, the scattering of a random periodic rough surface is computed in the absence of an object so that the periodic boundary condition can still be used to confine the computation domain in a finite region. The computation domain for this step is the same as that depicted in Fig. 2, and the MPSTD algorithm is employed to compute the near-zone field, which is the sum of the incident field and the scattered field from the rough surface. In the second step, a cylinder is placed below the rough surface and the near-zone field obtained in the first step is used together with the incident field to excite the buried cylinder and the interaction between the buried cylinder and the rough surface is taken into account. The computation domain is shown in Fig. 3, where the total field (TF) region is enclosed by *abef*, and the region outside *abef* is defined as the scattered field (SF) region. The dimensions of *abef* and *fecd* are the same as that of $a'b'e'f'$ and $f'e'c'd'$ depicted in Fig. 2, respectively, and the boundaries *ad*, *bc* and *fe* correspond to $a'd'$, $b'c'$ and $f'e'$ used in Fig. 2.

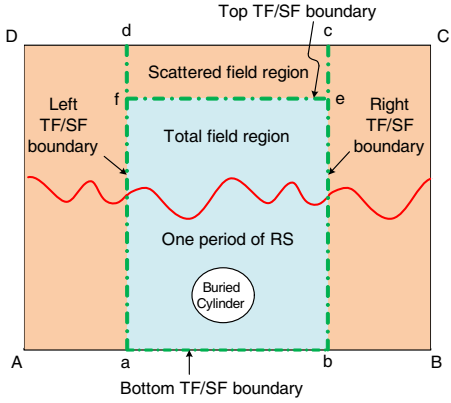

Figure 3. The computation domain for a cylinder buried below a random rough surface (The second step).

In the first step of the computation, the incident field is injected at the TF/SF boundary and the periodic boundary condition is enforced as illustrated in Fig. 2. The electromagnetic fields must satisfy the 2-D Maxwell's equations,

$$\begin{aligned} \frac{\partial H_x}{\partial t} &= -\frac{1}{\mu}\frac{\partial E_z}{\partial y}, \\ \frac{\partial H_y}{\partial t} &= \frac{1}{\mu}\frac{\partial E_z}{\partial x}, \\ \frac{\partial E_z}{\partial t} &= \frac{1}{\varepsilon}\left(\frac{\partial H_y}{\partial x} - \frac{\partial H_x}{\partial y}\right) - \frac{\sigma}{\varepsilon}E_z, \end{aligned} \tag{3}$$

under a TM_z plane wave incidence. This equation is solved numerically employing the MPSTD algorithm presented in [23–25]. In particular, the electromagnetic fields and their *spatial* derivatives appearing in Equation (3) are represented by a tensor-product Chebyshev-Lagarange polynomial. To take care of the *time* derivatives of the fields appearing in this equation, a Runge-Kutta method is employed for the time integration to advance the solution to the next time step. In the solution procedure, special attention is paid to the random rough surface, which is generated and treated as presented in the authors' previous work [25].

Then, the near-zone field obtained in step 1 is used together with the incident field in the second step as the excitation source to the buried cylinder, which is injected on the TF/SF boundaries. The sources introduced at the top and bottom TF/SF boundaries are the incident field used in step 1; the sources enforced at the left and right

boundaries are the near-zone field obtained in step 1. In this way, the near-zone field in the region enclosed by $a'b'c'd'$ from step 1 can be transported to the region enclosed by $abcd$ in step 2. The Maxwell's equations given in Equation (3) with the new excitation source are solved one more time employing the MPSTD algorithm. The field in the total field region enclosed by $abef$ is the sum of (a) the incident field, (b) the scattered field from the random periodic rough surface alone excited by the incident wave, (c) the scattering due to the buried cylinder excited by the near-zone field obtained in step 1, and (d) the scattering due to the interaction between the cylinder and the rough surface. The fields existing in the total-field and scattered-field regions in steps 1 and 2 are illustrated in Figs. 4(a) and 4(b). One notes that among the three components of the scattered fields, part (b) — the scattered field from the random periodic rough surface alone is indeed from the *entire* periodic structure due to the application of PBC based on Floquet theorem; and hence part (c) — the scattering from the buried cylinder is due to the excitation from the *entire* random periodic rough surface. Only part (d) — the interaction between the buried cylinder and the random periodic rough surface is an approximation — it is taken to be for one period of the rough surface that is right above the buried cylinder only; the interaction between the buried cylinder and the other parts of the rough surface is neglected due to the requirement that the computation domain must be finite. Therefore, it is important to have the length L of one period of the random periodic rough surface to be sufficiently large compared with the size of the buried cylinder so that the interaction between the cylinder and the other periods of the rough surface, which are at larger distances away from the cylinder, is weaker; and hence can be neglected as a good

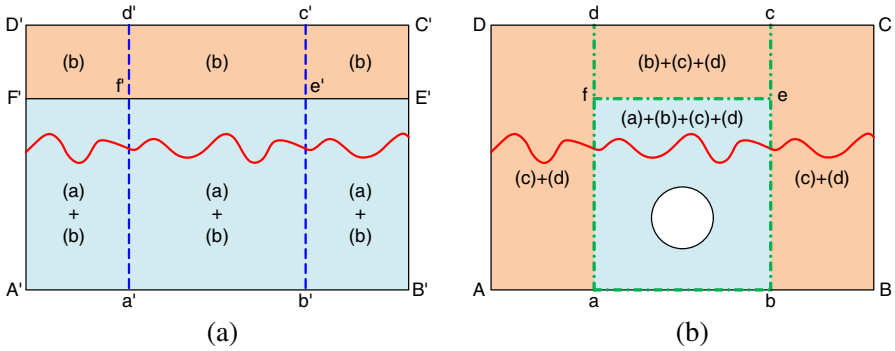

Figure 4. Illustration of the fields existing in the total-field and scattered-field regions. (a) In step 1. (b) In step 2.

approximation. This is to be demonstrated in a numerical example presented in Section 4. In addition, L must be much greater than the correlation length l_c to simulate the statistic characteristics of the roughness of a random rough surface as mentioned in Section 2.

Since the rough surface involved in this work has a random nature, a statistic average of the scattering needs to be determined by a Monte-Carlo procedure presented in [25]. First, a set of random rough surfaces with Gaussian spectrum is generated. Then, the two-step MPSTD algorithm formulated above is employed to determine the scattering of a buried cylinder below each of the rough surfaces generated. And finally, the statistic average of the scattering is determined after numerical tests to make sure that the result converges.

4. NUMERICAL RESULTS

Using the two-step approach formulated above, sample numerical results are obtained, presented, and validated in this section. For all the numerical results presented, the excitation is taken to be a normal TM_z plane wave incidence propagating in $-y$ direction, the time domain function of which is the first derivative of Blackmann-Harris window function with central frequency $f_c = 100\,\text{MHz}$. The random periodic rough surface is of period $L = 8\,\text{m}$ $(2.67\lambda_0)$ in parts (1) and (2) and of period $L = 10\,\text{m}$ $(3.33\lambda_0)$ in part (3); and the correlation length $l_c = 0.3\,\text{m}$ $(0.1\lambda_0)$, which satisfies the requirement $L \geq 15l_c$. It is of *rms* height $\sigma_{rms} = 0.3\,\text{m}$ $(0.1\lambda_0)$, unless otherwise specified. The medium above the rough surface is assumed to be free space and the medium below the rough surface is an isotropic, lossless medium with $\mu_r = 1$ and $\varepsilon_r = 3$, unless otherwise indicated. The incident wave is originated in the upper half space above the rough surface. The incident fields are the fields of the incident wave propagating in the absence of the rough surface and the buried cylinder. In all the computation domains presented in this section, the most outer subdomains are the PML regions. The statistic average of the scattering is taken for 15–18 realizations of the random rough surface after a series of numerical tests as described in [25] to make sure that the results converge.

4.1. Verification of the Periodic Boundary Condition and Validation of the Two-step Approach

In the first numerical example, we consider a random rough periodic surface alone. The computation domain is shown in Fig. 5(a), in which the total field region is the region $-6 \leq x \leq 6$, $-6 \leq y \leq 2$, and

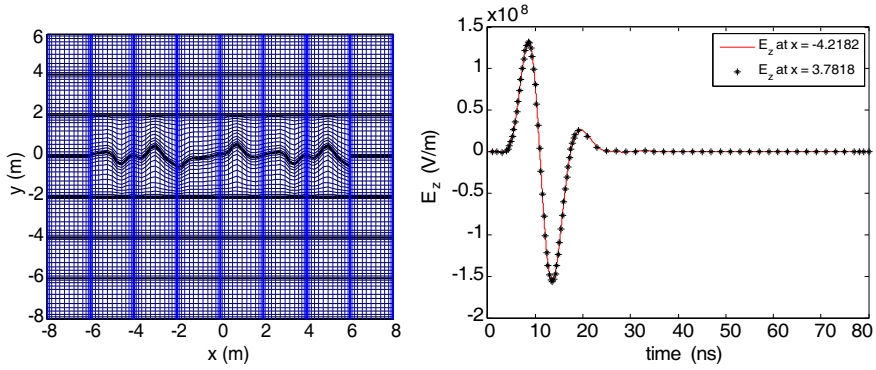

Figure 5. Scattering from a random periodic rough surface. (a) The computation domain. (b) Fields observed at two points separated by a period of the rough surface.

the scattered field exists in the region $-6 \leq x \leq 6,\ 2 \leq y \leq 4$. The left and right periodic boundaries are located at $x = -4$ and $x = 4$. The statistic average of 15 rough surface realizations is taken after a convergence test [25]. The numerical results are shown in Fig. 5(b) for the electric field observed at two different observation points $x = -4.2182$ and $x = 3.7818$ along $y = 1$, which are separated by a distance of the length of a period. From this figure, one sees that the fields at these two points are identical, which underlines that the resulting fields are indeed periodic after applying the periodic boundary condition.

The second example is devoted to validate the two-step MPSTD approach. Since there is not existing result in the literature for the same problem solved in this work, we employ the two-step approach to study a simpler geometry, which is a circular PEC cylinder buried below a random rough surface of finite length; and then compared the numerical results with published data. As shown in Fig. 6(a), the random rough surface exists in the region of $-4 \leq x \leq 4$; it becomes a flat interface for $x < -4$ and $x > 4$. The numerical results of the electric field E_z obtained by employing the two-step approach is observed at (0, 2) and compared with the published data [25]. From the comparison illustrated in Fig. 6(b), one sees that the two sets of data fall on top of each other.

4.2. Scattering from Random Periodic Rough Surface Alone

As a partial check of the two-step approach, in this section, we employ it to compute the fields due to a random periodic rough

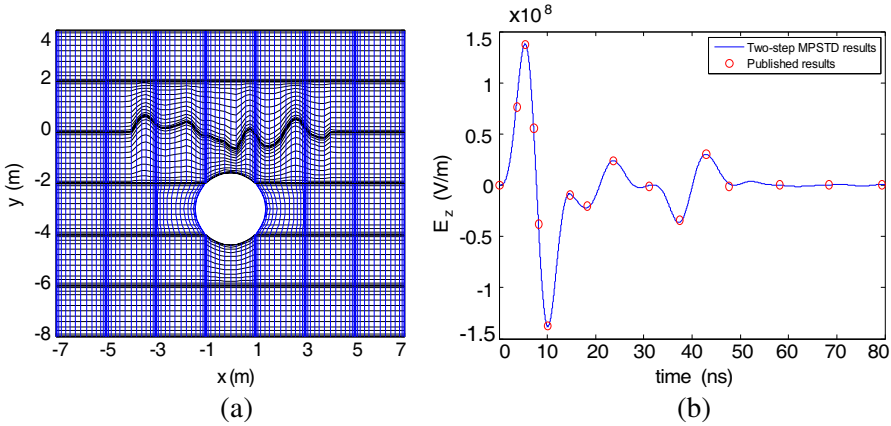

(a) (b)

Figure 6. Electric field at $(0, 2)$ for a circular PEC cylinder buried below a random rough surface of finite length. (a) The computation domain. (b) Comparison of the two-step MPSTD results with published datal.

surface, in absence of the buried cylinder, first. The geometry and the computation domain are the same as that illustrated previously in Fig. 5(a), hence it is not repeated here. The periodic boundaries are located at $x = -4$ and $x = 4$ in step 1 and the TF/SF boundaries are at $x = -4$ and $x = 4$ in step 2. Since there is no buried cylinder, one predicts that the field in the total field region obtained in step 2 should be the same as that obtained in step 1; and no field should be found in the scattered field region in step 2 since there is no scatterer.

Numerical results of *spatial* distribution of the electric field obtained at a specific moment $t = 20\,\text{ns}$ in step 1 and step 2 are shown in Figs. 7(a) and (b), respectively. The phenomena illustrated in the figures are exactly as what is predicted above. The near zone field obtained in step 1 is successfully transferred to step 2 and no field exists in the scattered field region. In addition, it is of interest to note that the field distribution presented in both figures well represent the shape of the rough surface depicted in Fig. 5(a).

Then, in Fig. 8, we present the same results but as a function of *time* observed at four observation points. At point (1, 1), which is in the total field region in both steps 1 and 2, the fields obtained in these two steps are exactly the same as expected. At $(-1, 3)$ that is in the scattered field region in step 1 and is in the top scattered field region enclosed by *fecd* in step 2, the two sets of data also fall on top of each other as they are supposed to be. At points $(-5, -5)$ and $(5, 1)$, which are in the total field region in step 1 but in the left and right scattered

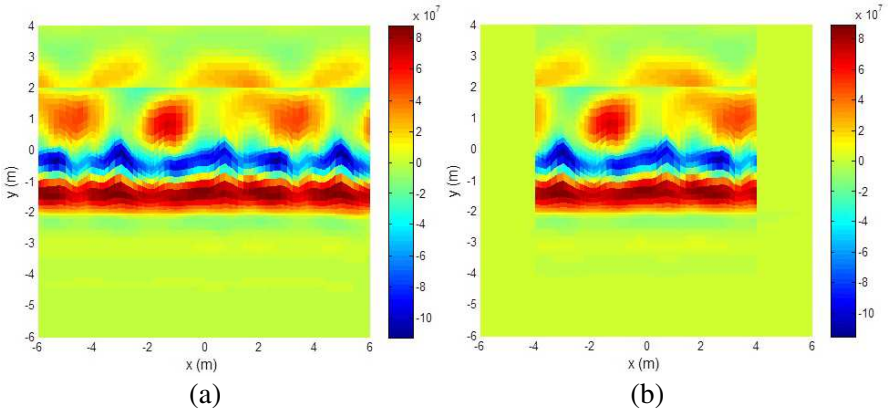

Figure 7. Spatial distribution of the electric field obtained at $t = 20\,\text{ns}$. (a) In step 1. (b) In step 2.

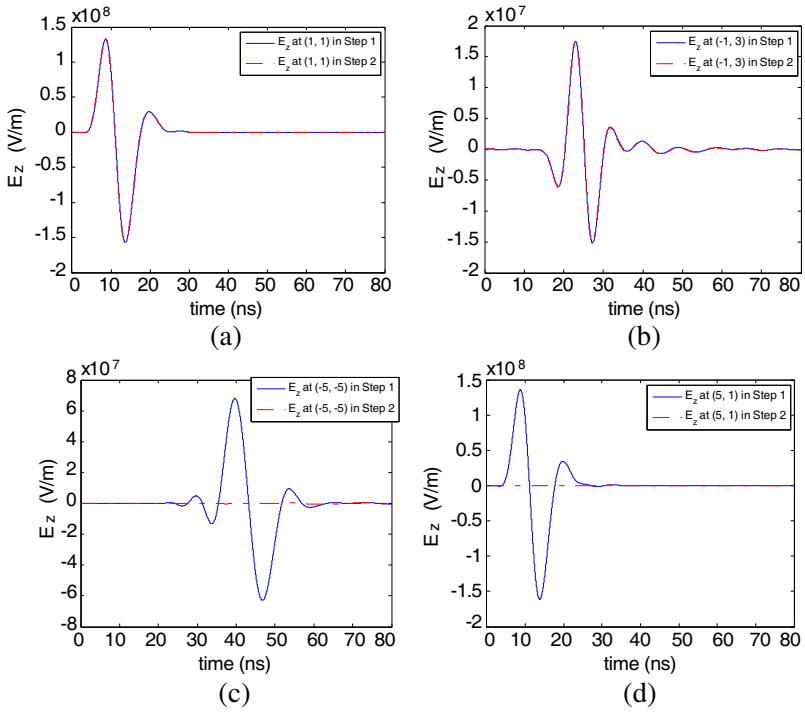

Figure 8. Electric field as a function of time observed at different points in step 1 and step 2.

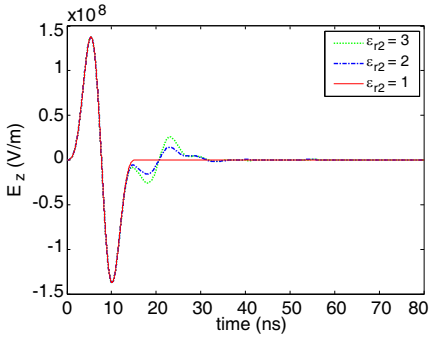

Figure 9. Electric field at $(0, 2)$ for different lower half-space relative permittivities.

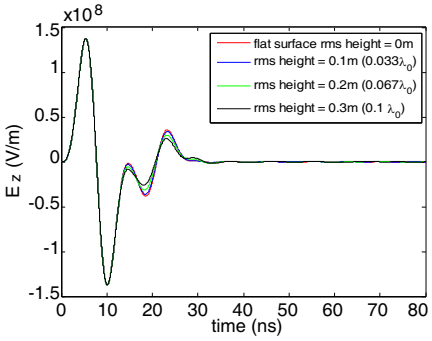

Figure 10. Electric fields at $(0, 2)$ for various *rms* heights of the rough surface.

field regions in step 2, the scattered field obtained in step 2 is zero as expected since there is no scatterer. The observations made above can serve as a partial check of the correctness of the numerical results.

Next, we present the numerical results corresponding to different lower half-space ε_{r2} and various *rms* height σ_{rms}. The results shown in Fig. 9 are for the electric fields observed at (0, 2) for $\varepsilon_{r2} = 3$, $\varepsilon_{r2} = 2$, and $\varepsilon_{r2} = 1$. From the data presented, one notes that the electric filed gradually reduces to that in free space as ε_{r2} varies from 3, to 2, then 1; as expected.

Figure 10 illustrates the numerical results of the electric field observed at (0, 2) for various *rms* heights of the random periodic rough surface, 0.3 m $(0.1\lambda_0)$, 0.2 m $(0.067\lambda_0)$, 0.1 m $(0.033\lambda_0)$ and for a flat surface. From this figure, one sees that the result of the field gradually converges to the analytical result for a flat surface ($\sigma_{rms} = 0$) as the *rms* height of the rough surface decreases from 0.3 to 0.2, to 0.1, and finally to 0, as it is supposed to be. The observations made on the two examples above can be used as a partial check of the correctness of their numerical results.

4.3. Scattering from Buried Cylinder below a Random Periodic Rough Surface

In the next a few examples, we present the numerical results of the scattering of a circular PEC cylinder buried below a random periodic rough surface. As indicated in the previous section, it is important to have the length L of one period of the random periodic rough surface to be sufficiently large compared with the size of the buried cylinder so

that the interaction between the cylinder and the other periods of the rough surface, which are at larger distances away from the cylinder, is weaker; and hence can be neglected as a good approximation. This is demonstrated in a numerical example presented below. As illustrated in Figs. 11(a), 11(b), and 11(c), a period of the rough surface right above the buried cylinder is located in $-5 \leq x \leq 5$ and the length of a period $L = 10\,\mathrm{m}$ remains unchanged; but the computation domain is taken to be of different lengths of $14\,\mathrm{m}$ $(-7 \leq x \leq 7)$, $18\,\mathrm{m}$ $(-9 \leq x \leq 9)$, and $22\,\mathrm{m}$ $(-11 \leq x \leq 11)$. The numerical results of the electric field observed at $(0,\ 2)$, $(-3, 2)$, and $(-4, 2)$ are presented in Figs. 11(d), 11(e), and 11(f), respectively; and in each of these three figures, the numerical results for the different computation domain lengths are compared with each other. The comparisons show that increasing the computation domain length beyond the period right above the buried cylinder has little effect on the numerical results. This demonstrates that the length of the period of the random periodic surface considered in the computation is sufficiently large so that the interaction between the buried cylinder and the other periods of the rough surface ($x < -5$ and $x > 5$) can indeed be neglected and the total length of the rough surface included in the finite computation domain is adequate; hence verifies that the two-step MPSTD approach

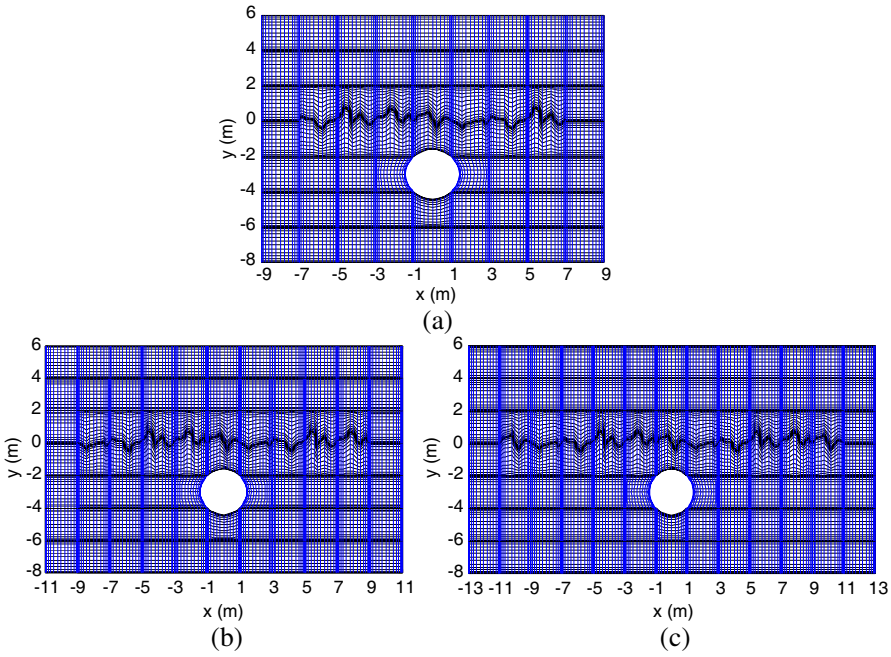

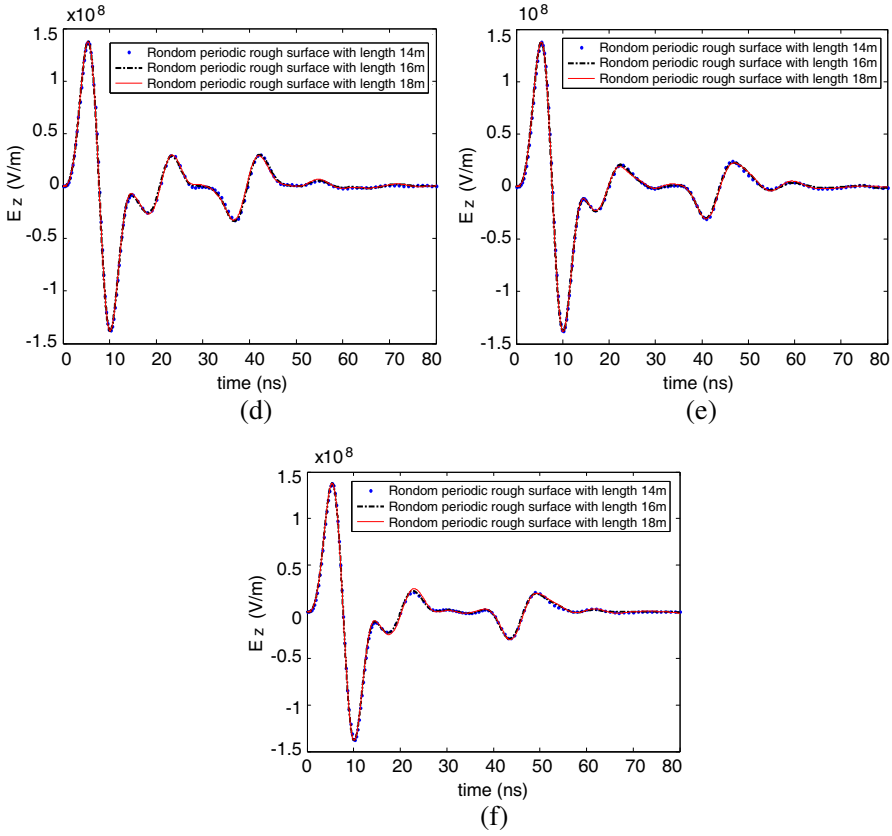

Figure 11. Comparison of the numerical results for different computation domain lengths. (a) Computation domain of length of 14 m, (b) 18 m, (c) 22 m. (d) Comparison of the results at $(0, 2)$, (e) at $(-3, 2)$, (f) at $(-4, 2)$.

presented in Section 3 works effectively for a random periodic rough surface with a period of sufficiently large length.

In addition, numerical tests have been performed to verify the effectiveness of the two-step approach as L increases. The results of the numerical tests show that using a laptop with an Intel Core i3 CPU processor, the CPU time needed for one realization is 10 minutes for $L = 10$ m and is 14 minutes as L is increased to 14 m. From the limited CPU time increase, it is expected that the two-step MPSTD method can also effectively work well for larger L.

Then, the spatial distributions of the electric field, for the configuration depicted in Fig. 11(a), obtained at $t = 20$ ns, 26 ns, and

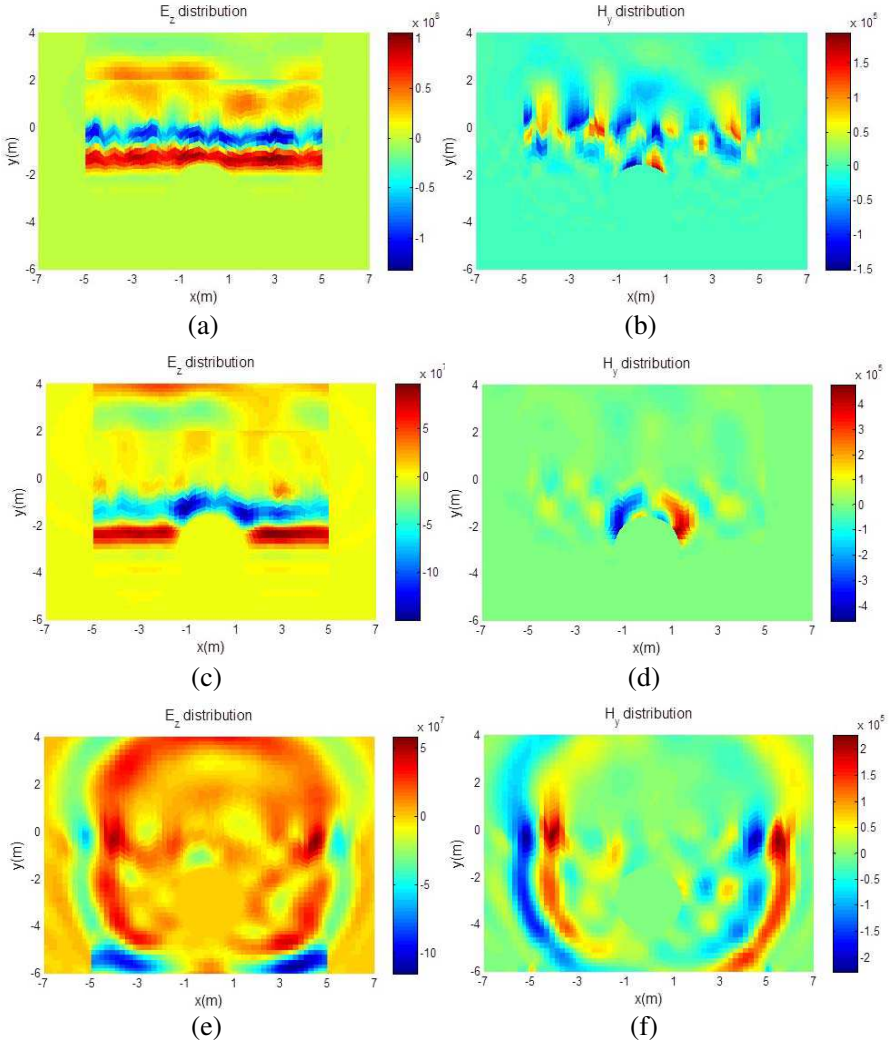

Figure 12. Spatial distribution of the fields obtained at different moment. (a) E_z at $t = 20$ ns, (b) H_y at $t = 20$ ns, (c) E_z at $t = 26$ ns, (d) H_y at $t = 26$ ns, (e) E_z at $t = 50$ ns, (f) H_y at $t = 50$ ns.

50 ns are shown in Figs. 12(a), (c), and (e); and the corresponding magnetic field distributions are depicted in Figs. 12(b), (d), and (f). It is of interest to observe that the electric field distribution obtained at $t = 20$ ns shown in Fig. 12(a) clearly illustrates the shape of the random rough surface but it only depicts a portion of the buried cylinder.

This is due to the fact that the incident field hits the random rough surface first and then the buried cylinder; and at $t = 20\,\text{ns}$ only a portion of the cylinder is illuminated by the incident wave. But as time progresses, the incident wave travel farther in the lower half space. At $t = 26\,\text{ns}$, the scattering from the random rough surface as well as the buried cylinder appears in the left and right scattered field region. At $t = 50\,\text{ns}$, the incident field covers the whole buried cylinder and hence its complete shape is well illustrated in Figs. 12(e) and (f), as expected.

As a partial check, next, we present the numerical results of the scattering corresponding to different relative permittivity ε_{r2} of the lower half space. As shown in Fig. 13(a), ε_{r2} can significantly alter the scattering, and as it changes from 3, to 2, then to 1.01, and finally to 1, the result converges to that in free space, which perfectly matches the analytic result [35] presented in Fig. 13(b), as it is supposed to be.

Another partial check is performed by comparing the numerical result of the electric field obtained at (0, 2), which is in the middle of a period L of the random periodic rough surface with $L = 10\,\text{m}$ as depicted in Fig. 11(a), with that observed at the same point for a random rough surface of finite length L, beyond the two ends of which is a flat interface ($x < -5$ and $x > 5$) that is not a periodic structure. For a sufficiently large L compared with the dimension of the buried cylinder it is expected that the two results should be about the same. This is exactly what is illustrated in Fig. 14.

Next, we compare the two sets of data at a different point (4.434, 2), which is close to the right end of a period of the random periodic rough surface. The comparison presented in Fig. 15 shows a significance difference (the maximum difference is about 110%) of the

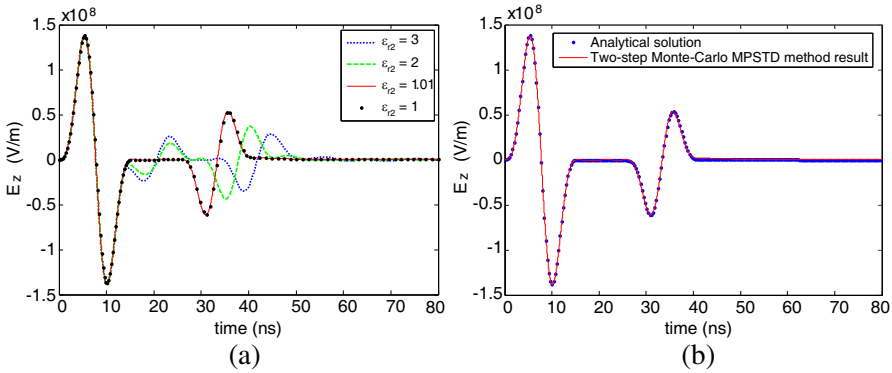

Figure 13. (a) E_z observed at (1, 2) for various ε_{r2}. (b) Comparison of the numerical result with analytical solution for $\varepsilon_{r2} = 1$.

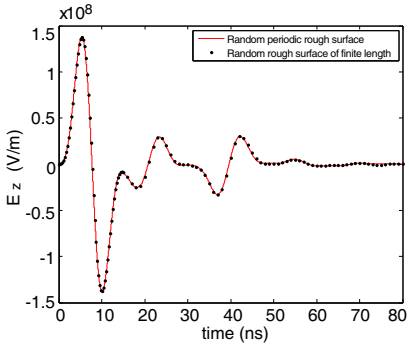

Figure 14. Comparison of E_z at the middle point (0, 2) of a period of arandom periodic rough surface with that for a random rough surface of finite length.

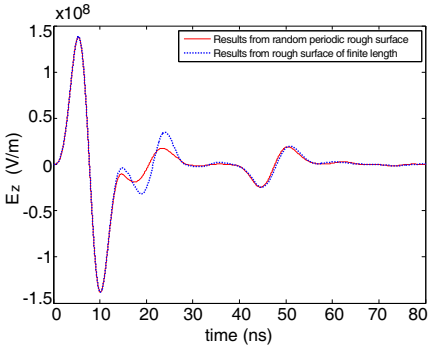

Figure 15. Comparison of E_z at (4.434, 2) near the end point of a period of a random periodic rough surface with that for a random rough surface of finite length.

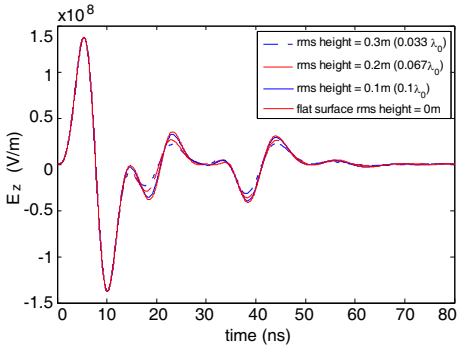

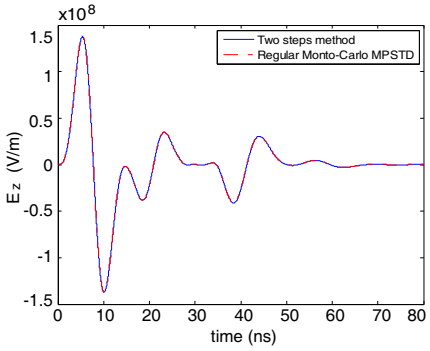

Figure 16. (a) E_z observed at $(-3, 2)$ for various σ_{rms}. (b) Comparison of the results obtained by two different methods for a flat interface.

scattering corresponding to the random periodic rough surface and that of finite length. This is due to the fact that the scattering observed at a point near the end of a period contains the contribution from the adjacent period of the rough surface, which does not exist for a random rough surface of finite length. Such a significance difference between the two sets of numerical results indicates that it is necessary to extend the analysis of scattering involving a random rough surface of finite length to cover the more realistic case, in which a random

periodic rough surface is considered.

In Fig. 16, the numerical results of the electric field corresponding to various *rms* height σ_{rms} of the random rough surface are presented. As illustrated in Fig. 16(a), when σ_{rms} varies from 0.3, to 0.2, then to 0.1, and finally to 0, the result converges to that for a flat media interface. Furthermore, as shown in Fig. 16(b), the results obtained by the two-step approach for the flat interface is exactly the same as that got from the "regular" Monte-Carlo MPSTD algorithm presented in [25] as expected.

The two-step Monte-Carlo MPSTD numerical technique developed in this work can be employed for determining the scattering of a cylinder of arbitrary shape buried below a random periodic rough surface. The last sample numerical result is for the scattering of a

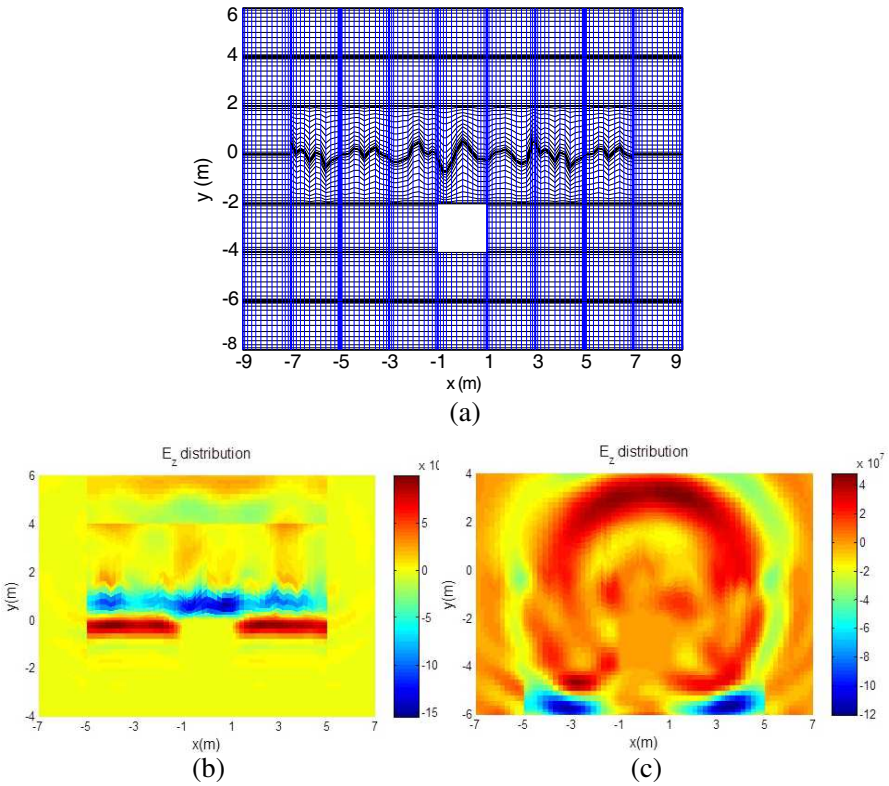

Figure 17. Spatial distribution of E_z obtained at different moments. (a) Geometry and computation domain. (b) E_z at $t = 25\,\text{ns}$, (c) E_z at $t = 50\,\text{ns}$.

rectangular PEC cylinder of dimension $2\,\mathrm{m} \times 2\,\mathrm{m}$ $(0.67\lambda_0 \times 0.67\lambda_0)$ with its axis along $(0, -3)$, buried below a random periodic rough surface. The geometry and computation domain with grids are depicted in Fig. 17(a). In Figs. 17(b) and (c), the spatial distributions of E_z at two moments $t = 25\,\mathrm{ns}$ and $t = 50\,\mathrm{ns}$ are presented. Similar to what has been seen in Fig. 12, one observe that the electric field distribution obtained at $t = 25\,\mathrm{ns}$ shown in Fig. 17(b) illustrates the shape of the random rough surface but it only depicts a portion of the buried rectangular cylinder. This is due to the fact that the incident field hits the random rough surface first and then the buried cylinder; and at $t = 25\,\mathrm{ns}$ only a portion of the cylinder is illuminated by the incident wave. But as time progresses, the incident wave travel farther in the lower half space. At $t = 50\,\mathrm{ns}$, the incident field covers the whole buried rectangular cylinder and hence its complete shape is well illustrated in Fig. 17(c).

5. CONCLUSIONS

A two-step Monte-Carlo MPSTD numerical technique is developed and implemented for the analysis of scattering of a cylinder buried below a random periodic rough surface. In addition to the advantages of the MPSTD technique over the traditional FDTD method mentioned in the section of "Introduction", the benefit of using the two-step approach is described as the follows. As shown in Section 3, after placing a cylinder below the random periodic rough surface, the structure is no longer periodic and the periodic boundary condition (PBC) does not hold any more, hence it is hard to solve this problem within a finite computation domain. To overcome this difficulty, we decompose the solution of this complicated problem into two steps. In the first step, only the random rough surface is considered so that the PBC still holds and hence can be enforced to simulate the entire random periodic rough surface by only one period of the rough surface contained in a finite computation domain. Then, in the second step, the near-zone field obtained in the first step is used together with the incident field as the excitation source to the buried cylinder to determine the electromagnetic fields taking into account the scattering of the buried cylinder as well as the interaction between the buried cylinder and the rough surface. As explained in Section 3 and demonstrated in Section 4, for a sufficiently large length L of one period of the random periodic rough surface, the computation domain can still be confined in a finite region. In this way, taking the two-step MPSTD approach, the difficulty caused by placing a buried cylinder below a periodic rough surface has been overcome and the computation

can be carried out effectively without losing its accuracy.

To extend the combination of the two-step MPSTD technique with the Monte-Carlo analysis presented in this paper, the authors are currently studying the scattering of a cylinder embedded in a layered half space with random rough interfaces, which may more faithfully simulate the real earth and thus has a potential of both civil and military applications including subsurface investigations and target detections.

ACKNOWLEDGMENT

The authors appreciate the financial support provided by the National Science Foundation to this work, under award number 0821918. Also, the authors thank Profs. Q. H. Liu and Y. Chen for helpful technical discussions. Special thanks from the authors go to Prof. Y. Shi and Dr. G. X. Fan for their helpful suggestions/comments during numerous detailed technical discussions.

REFERENCES

1. Lawrence, D. E. and K. Sarabandi, "Electromagnetic scattering from a dielectric cylinder buried beneath a slightly rough surface," *IEEE Transactions on Antennas and Propagation*, Vol. 50, No. 10, 1368–1376, Oct. 2002.
2. Johnson, J. T. and R. J. Burkholder, "Coupled canonical grid/discrete dipole approach for computing scattering from objects above or below a rough interface," *IEEE Transactions on Geoscience and Remote Sensing*, Vol. 39, No. 6, 1214–1220, Jun. 2001.
3. Johnson, J. T. and R. J. Burkholder, "A study of scattering from an object below a rough surface," *IEEE Transactions on Geoscience and Remote Sensing*, Vol. 42, No. 1, 59–66, Jan. 2004.
4. El-Shenawee, M., "Scattering from multiple objects buried beneath two-dimensional random rough surface using the steepest decent fast multipole method," *IEEE Transactions on Antennas and Propagation*, Vol. 51, No. 4, 802–809, Apr. 2003.
5. El-Shenawee, M., "Polarimetric scattering from two-layered two-dimensional random rough surfaces with and without buried objects," *IEEE Transactions on Geosciences and Remote Sensing*, Vol. 42, No. 1, 67–76, Jan. 2004.
6. El-Shenawee, M., C. Rappaport, E. Miller, and M. Silevitch, "3-D subsurface analysis of electromagnetic scattering from

penetrable/PEC objects buried under rough surface: Use of the steepest descent fast multipole method (SDFMM)," *IEEE Transactions on Geoscience and Remote Sensing*, Vol. 39, 1174–1182, Jun. 2001.

7. El-Shenawee, M., C. Rappaport, and M. Silevitch, "Monte Carlo simulations of electromagnetic scattering from random rough surface with 3-D penetrable buried objects: Mine detection application using the SDFMN," *Journal of Optical Society America A*, Dec. 2001.
8. Kuo. C. and M. Moghaddam, "Electromagnetic scattering from a buried cylinder in layered media with rough interfaces," *IEEE Transactions on Antennas and Propagation*, Vol. 54, No. 8, 2392–2401, Aug. 2006.
9. Duan, X. and M. Moghaddam, "Vector electromagnetic scattering from layered rough surfaces with buried discrete random media for subsurface and root-zone soil moisture sensing," *Proceedings of IEEE International Geosciences and Remote Sensing Symposium*, 1227–1230, Jul. 2011.
10. Ozgun, O. and M. Kuzuoglu, "Monte Carlo-based characteristic basis finite-element method (MC-CBFEM) for numerical analysis of scattering from objects on/above rough sea surface," *IEEE Transactions on Geoscience and Remote Sensing*, Vol. 50, No. 3, 769–783, Mar. 2012.
11. Kuang, L. and Y.-Q. Jin, "Bistatic scattering from a three-dimensional object over a randomly rough surface using the FDTD algorithm," *IEEE Transactions on Antennas and Propagation*, Vol. 55, No. 8, 2302–2312, Aug. 2007.
12. Dridi, K. H., J. S. Hesthaven, and A. Ditkowski, "Staircase-free finite-difference time-domain formulation for general materials in complex geometries," *IEEE Transactions on Antennas and Propagation*, Vol. 49, No. 5, 749–756, May 2001.
13. Hastings, F. D., J. B. Schneider, and S. L. Broschat, "A finite-difference time-domain solution to scattering from a rough pressure-release surface," *Journal of the Acoustical Society of America*, Vol. 102, No. 6, 3394–3400, 1997.
14. Yang, B., D. Gottlieb, and J. S. Hesthaven, "Spectral simulation of electromagnetic wave scattering," *Journal of Computational Physics*, Vol. 134, 216–230, 1997.
15. Yang, B. and J. S. Hesthaven, "A pseudospectral method for time-domain computation of electromagnetic scattering by bodies of revolution," *IEEE Transactions on Antennas and Propagation*, Vol. 47, No. 1, 132–141, Jan. 1999.

16. Zhao, G. and Q. H. Liu, "The 2.5-D multidomain pseudospectral time-domain algorithm," *IEEE Transactions on Antennas and Propagation*, Vol. 51, No. 3, 619–627, Mar. 2003.
17. Zhao, G. and Q. H. Liu, "The 3-D multidomain pseudospectral time-domain algorithm for inhomogeneous conductive media," *IEEE Transactions on Antennas and Propagation*, Vol. 52, No. 3, 559–562, Jun. 22–27, 2003.
18. Shi, Y. and C.-H. Liang, "A strongly well-posed PML with unsplit-field formulations in cylindrical and spherical coordinates," *Journal of Electromagnetic Waves and Applications*, Vol. 19, No. 13, 1761–1776, 2005.
19. Shi, Y. and C. -H. Liang, "Two dimensional multidomain pseudospectral time-domain algorithm based on alternating-direction implicit method," *IEEE Transactions on Antennas and Propagation*, Vol. 54, No. 4, 1207–1214, Apr. 2006.
20. Shi, Y. and C.-H. Liang, "Multidomain pseudospectral time domain algorithm using a symplectic integrator," *IEEE Transactions on Antennas and Propagation*, Vol. 55, No. 2, 433–439, Feb. 2007.
21. Shi, Y. and C.-H. Liang, "Characteristic variables patching conditions in multidomain pseudospectral time domain," *IEEE Antennas and Wireless Propagation Letters*, Vol. 6, 353–356, 2007.
22. Liu, Q. H., "The PSTD algorithm: A time-domain method requiring only two cells per wavelength," *Microwave and Optical Technology Letters*, Vol. 15, No. 3, 158–165, Jun. 20, 1997.
23. Fan, G. X., Q. H. Liu, and J. S. Hesthaven, "Multidomain pseudospectral time-domain simulations of scattering by objects buried in lossy media," *IEEE Transactions on Geoscience and Remote Sensing*, Vol. 40, No. 6, 1366–1373, Jun. 2002.
24. Taflove, A. and S. C. Hagness, *Computational Electrodynamics The Finite-difference Time-domain Method*, 3rd Edition, Chapter 17, Advances in PSTD Techniques, by Q. H. Liu and G. Zhao, Artech House, Inc., Norwood, MA, 2005.
25. Liu, W., Y. Dai, H. Yang, and X.-B. Xu, "Scattering of object buried below random rough surface — A Monte-Carlo pseudospectral time-domain approach," *Electromagnetics*, Vol. 32, No. 6, 330–344, Aug. 2012.
26. Tsang, L., J. A. Kong, K. H. Ding, and C. O. Ao, *Scattering of Electromagnetic Waves, (Volume II) Numerical Simulations*, John Wiley & Sons Inc., New York, 2001.
27. Ye, H. and Y. Q. Jin, "Parameterization of the tapered incident wave for numerical simulation of electromagnetic scattering from

rough surface," *IEEE Transactions on Antennas and Propagation*, Vol. 53, No. 3, 1234–1237, Mar. 2005.

28. Chan, C. H., S. H. Lou, L. Tsang, and J. A. Kong, "Electromagnetic scattering of waves by random rough surface: A finite-difference time-domain approach," *Microwave and Optical Technology Letters*, Vol. 4, No. 9, 355–359, Aug. 1991.
29. Veysoglu, M. E., R. T. Shin, and J. A. Kong, "A finite-difference time-domain analysis of wave scattering from periodic surface: Oblique incidence case," *Journal of Electromagnetic Waves and Applications*, Vol. 7, No. 12, 1595–1607, 1993.
30. Tsay, W. J. and D. M. Pozar, "Application of the FDTD technique to periodic problems in scattering and radiation," *IEEE Microwave and Guided Wave Letters*, Vol. 3, No. 8, 250–252, Aug. 1993.
31. Yang, F., J. Chen, R. Qiang, and A. Elsherbeni, "FDTD analysis of periodic structures at arbitrary angles: A simple and efficient implementation of the periodic boundary conditions," *Proceedings of IEEE Antennas and Propagation Society International Symposium*, 2715–2718, 2006.
32. Wong, P. B., G. L. Tyler, J. E. Baron, E. M. Gurrola, and R. A. Simpson, "A three-wave FDTD approach to surface scattering with applications to remote sensing of geophysical surfaces," *IEEE Transactions on Antennas and Propagation*, Vol. 44, No. 4, 504–514, Apr. 1996.
33. Zhu, X. and L. Carin, "Multiresolution time-domain analysis of plane-wave scattering from general three-dimensional surface and subsurface dielectric targets," *IEEE Transactions on Antennas and Propagation*, Vol. 48, No. 11, 1568–1578, Nov. 2001.
34. Yi, Y., B. Chen, D.-G. Fang, and B.-H. Zhou, "A new 2-D FDTD method applied to scattering by infinite objects with oblique incidence," *IEEE Transactions on Electromagnetic Compatibility*, Vol. 47, No. 4, 756–762, Nov. 2005.
35. Harrington, R. F., *Time-Harmonic Electromagnetic Fields*, IEEE Press, 2001.